Terahertz Conductivity of Silver Nanowire Layers

Aleksandra Przewloka
Institute of High Pressure Physics
Serguei Smirnov
Royal Institute of Technology
Irina Nefedova
Aalto University
Aleksandra Krajewska
Institute of High Pressure Physics
Igor Nefedov
Peoples' Friendship University of Russia
Petr Demchenko
ITMO University
Dmitry Zykov
ITMO University
Valentin Chebotarev
ITMO University
Dmytro But
Institute of High Pressure Physics
Kamil Stelmaszczyk
Institute of High Pressure Physics
Alvydas Lisauskas
Vilnius University
Joachim Oberhammer
Royal Institute of Technology
Mikhail Khodzitsky
ITMO University
Wojciech Knap
Institute of High Pressure Physics
Dmitri Lioubtchenko (dml@kth.se)
Institute of High Pressure Physics

Research Article

Keywords: Terahertz, silver nanowire, AgNWs

Posted Date: June 14th, 2021

DOI: https://doi.org/10.21203/rs.3.rs-595367/v1

Terahertz conductivity of silver nanowire layers

Aleksandra Przewłoka[1,2], Serguei Smirnov[3], Irina Nefedova[4], Aleksandra Krajewska[1], Igor S. Nefedov[5], Petr S. Demchenko[6], Dmitry V. Zykov[6], Valentin S. Chebotarev[6], Dmytro B. But[1], Kamil Stelmaszczyk[1], Alvydas Lisauskas[1,7], Joachim Oberhammer[3], Mikhail K. Khodzitsky[6], Wojciech Knap[1], and Dmitri V. Lioubtchenko[1,3,*]

[1]CENTERA Laboratories, Institute of High-Pressure Physics PAS, 01-142 Warsaw, Poland
[2]Institute of Optoelectronics, Military University of Technology, 00-908 Warsaw, Poland
[3]Department of Micro and Nanosystems, KTH Royal Institute of Technology, SE-100 44 Stockholm, Sweden
[4]Department of Electronics and Nanoengineering, Aalto University, School of Electrical Engineering, Finland
[5]People's Friendship University of Russia (RUDN University), 117198 Moscow, Russian Federation
[6]THz Biomedicine Laboratory, ITMO University, 197101 Saint Petersburg, Russian Federation
[7]Institute of Applied Electrodynamics and Telecommunications, Vilnius University, 10257 Vilnius, Lithuania
[*]e-mail: dml@kth.se

ABSTRACT

We present the study of the influence of different thin silver nanowire layers on electrical and optical properties in the Terahertz (THz) frequency range. We demonstrate that the absorbance, transmittance and reflectance of the metal nanowire layers in the frequency range of 0.2 THz to 1.2 THz is non-monotonic and depends on the nanowire dimensions and density. We present and validate also a theoretical approach describing well the experimental results and allowing to model the THz response as function the nanowire layer structure. Our results pave the way toward the application of silver nanowires as a perspective material for transparent and conductive coatings, and printable antennas operating in the terahertz range – significant for future wireless communication devices.

Introduction

Rapid digitization of the world results in higher and higher expectations for the electronics industry.[1] In particular, the attention is focused on the new group of electronic devices,which are expected to transfer information with speeds going up to hundreds of Gigabits per second. For this reason, high hopes are pinned on terahertz (THz) radiation that can carry high data rates with simplified modulation schemes. The THz frequency range became the subject of intense research only in the 1990s.[2,3] This has been caused by difficulties with designing devices capable of generating, detecting, and modulating the signals.[2,4] The fast development of technology in various fields has opened new doors for broad applications of THz radiation, not only for wireless high data rate communication but also in medical diagnosis, imaging techniques, non-destructive testing, security screening, sensing of contamination in water, food and medicines.[3,5–9]

The conventional techniques that are currently used in antenna manufacturing cannot fulfil the growing expectations of certain emerging applications which require antennas with high transparency and flexibility.[1] To address this issue, the present research focuses on implementing functional materials, e.g., graphene,[10–12] carbon nanotubes,[8,13] and metallic nanostructures,[14–21], for the design of miniaturized and tunable antennas. The conductivity of the metal defines the antenna performance, such as radiation efficiency.[22] In metal nanowire networks, adjusting the length, diameter, and concentration of wires allows adjustment of the optical/THz properties that may lead to improvement of the efficiency of nanowire-based antennas.[14,18,23,24]

Metal nanowires, especially silver nanowires (AgNWs), are a perspective material for nanoelectronic circuits, transparent and conductive coatings, printable antennas, and other applications.[22,25–30] There are numerous reports on the fabrication of AgNW layers, such as vacuum filtration,[31,32] transfer printing,[33–35],, air-spraying from suspension,[36,37] and rod-coating technique.[38,39] Nevertheless, all of these methods present several challenges related to the inability to obtain layers that would simultaneously exhibit excellent high frequency/THz properties, low surface roughness, high transparency, flexibility, and stretchability.[35,40] The direct deposition of AgNW layers by printing seems to be the most attractive and promising technique due to its advantages, such as low cost, the facility of production,and the feasibility of large-scale integration.[33,41]

One of the AgNW layers' essential characteristic (which is crucial for THz antennas and reflective surfaces) is that they can keep relatively high and frequency independent conductivity in a wide frequency range.[14,36]

It has been demonstrated that AgNW films with relatively high optical transparency are suitable for plasmonic devices

operating in the THz range.[25] Also, a hybrid THz slot antenna based on a AgNWs network film was described as a promising device for an extremely sensitive microbial detection.[22] The characterization of nano-sized materials in 2D layers is a challenging problem. The reflection/transmission measurement based on the Nicolson-Ross-Weir parameter extraction algorithm is the most commonly used characterization method.[42] There are also various methods based on cavities and open resonators.[43] These methods, however, are problematic when applied to very thin and lossy materials. In this article, we present the fabrication of thin silver nanowire layers of various diameters and lengths, with controlled surface densities. Except for the standard characterization methods (AFM, UV-Vis-IR spectroscopy), we also present systematic transmission and reflectivity measurements in the THz range (0.2 THz to 1.2 THz) with two different systems: pulsed time-domain spectroscopy (TDS) and continuous-wave (CW) frequency-domain spectroscopy. The experimentally observed dependencies are described by establishing the relation between the nanowire layer structure and the composite's electromagnetic response. Modified Drude-Smith model of conductivity indicate that the samples with a low density of nanowires follow the Drude-Smith model with a backscattering coefficient close to -1, and samples with a high density form a semi-continuous metallic layer. Our results indicates that silver nanowires are perspective material for nanoelectronic circuits, transparent and conductive coatings, and printable antennas operating in the terahertz range –significant for 5G and beyond, wireless communications.

Experimental

Sample preparation

The samples were prepared from commercial AgNWs in isopropanol (IPA) suspension (Sigma-Aldrich, 5 mg/ml) with three nanowire dimensions, detailed in Table 1 the volume equal to 100 μl of the AgNW-IPA suspension was next added to 300 ml of deionized H_2O and mixed in an ultrasonic bath for 30 minutes. Uniformly distributed AgNW layers were obtained by vacuum filtration of the diluted suspension with volumes ranging from 2 ml to 30 ml onto polyvinylidene difluoride membranes (Millipore HVLP, 0.45 μm pore size, 25 mm diameter, 125 μm thickness). The samples were dried in air and stored in N2 to avoid degradation of the nanowires.[27]

Sample	Diameter (nm)	Length (μ m)
A	40 ± 5	35 ± 5
B	35 ± 5	25 ± 5
C	30 ± 5	20 ± 3

Table 1. Nanowire dimensions

Sample characterization

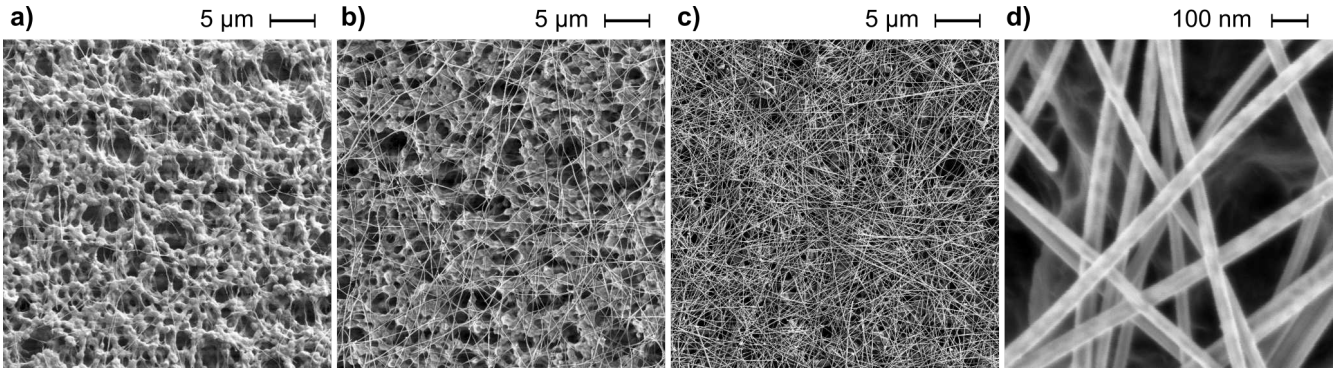

Figure 1. SEM images of AgNWs C samples with a) lowest sample density, showing individual nanowires and the morphology of the porous substrate, b) intermediate sample density at the percolation threshold, where the nanowires form a connected network, c) highest sample density with the nanowires forming a semi-continuous metallic layer, d) high magnification of c).

Scanning electron microscope (SEM) imaging was performed with a high-resolution SEM Zeiss Ultra 55. Fig. 1 shows typical SEM images of the AgNW layers with increasing densities from a) individual nanowires on the porous substrate, b) an interconnected nanowire network at approximately the percolation threshold, to c) a dense nanowire layer forming a continuous network. Only sample C is illustrated in Fig. 1 samples A and B were without any visual differences in the SEM figures.

Atomic force microscopy (AFM) was performed with a Veeco Dimension 5000 system. A typical AFM image of the AgNWs on a PET substrate is shown in Fig.S1. From the SEM and AFM images, the samples' thicknesses were estimated to range from an individual nanowire to a thick, dense layer: approximately between 50 nm and 1 μm. The optical transmittance spectra were obtained with a Perkin Elmer UV-Vis-NIR Lambda 1050+ spectrometer in the wavelength range of 300 nm to 800 nm. The optical absorbance of the samples in solution is shown in Fig. 2, with a well-known, characteristic strong peak at 375 nm originating from the transverse plasmon resonance of the nanowires.[27]

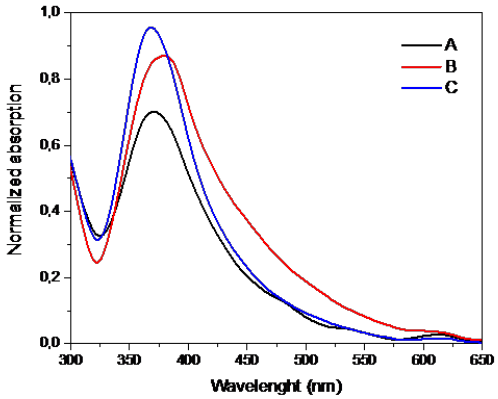

Figure 2. Optical absorbance of the three AgNW sample suspensions.

Terahertz time-domain spectroscopy

A terahertz TDS was used in transmission mode to extract the complex conductance of the AgNWs. An infrared femtosecond laser generates a series of pulses with a 1040 nm central wavelength, 200 fs pulse duration, 70 MHz repetition rate, and 15 nJ pulse energy. The laser beam is split into a probe beam and a pump beam with an energy ratio of 10% to 90%. The path of the pump beam is controlled by an optical delay line and modulated by a chopper at 667 Hz. The THz radiation is generated in an InAs crystal (in a magnetic field of 2 T). After passing through an IR filter, the THz beam incidents on the sample and reaches the CdTe semiconductor detector. The probe beam passes through a half-wave plate, a Glan prism, and meets with the THz beam on the CdTe surface. The polarization of the probe beam varies proportionally to the THz wave amplitude at a given time point, depending on the position of the time delay line. The beam is split into two orthogonally polarized components by a Wollaston prism and detected with balanced photodiodes. The schematic diagram ofthe THz TDS setup is illustrated in Fig.S3. A signal to noise ratio of 45 dB is achieved over the frequency range of 0.1 THz to 1 THz. The measurements were carried out at a temperature of 18.0 ± 0.4°C and relative humidity of 55.0%. The sample area under study was a circle of a diameter of 5 mm.

Terahertz frequency-domain spectroscopy

A commercial continuous-wave terahertz spectrometer (Toptica TeraScan 1550) was used for the frequency-domain measurements of the samples. The CW-THz spectrometer contains two distributed-feedback diode lasers (laser 1 and laser 2) working in the system using the photomixing technique, where the generated THz signal is equal to the frequency of the laser heterodyne.[44] Scanning of the THz frequency is achieved by cooling one while heating the other laser, which tunes the wavelength around the central value of 1.5 μm. Both lasers are combined to the beating signal via a 50:50 fibre coupler. The beating signal is split into the emitter (Tx) and the receiver (Rx) branch. The beat can be varied continuously from 0 to 1.2THz, with a practical lower limit of the setup around 50 GHz.[45] The laser beating signal is transformed via a self-complementary broadband antenna on InGaAs photodiode into a terahertz wave.43 The photomixers are placed on a hyper-hemispherical silicon lens, which suppresses back-reflections and pre-collimates the THz radiation in free space. The emitter is gated with a DC signal bias and a modulation AC lock-in signal. The receiver is connected to a lock-in signal amplifier. The bare substrate without nanowires and a silicon wafer were measured for reference.A schematic diagram of the system is illustrated in Fig.S4. The THz quasi-optical feed consists of four parabolic mirrors that can be configured in transmission or reflection with an incident angle of approx 10 degrees. The system achieves a peak dynamic range of 90 dB at 200 GHz (see Fig.S5) and a spectral resolution of 2 GHz.

Results and discussion

Time-domain waveforms of the THz pulses transmitted through the samples (AgNWs on the substrate), the bare substrate, and air as a reference are shown in Fig.S5. The amplitude and phase as a function of the frequency were calculated by fast Fourier transform (FFT) of the time-domain pulses. For the CW system, the amplitude spectrum was obtained from the measured frequency-domain photocurrent (see Fig.S6). The amplitude of each local maximum was averaged with the adjacent minimum to remove DC offsets in the photocurrent and was linearly interpolated to the original frequency point.The transmittance for both systems was obtained as the ratio of amplitudes through the samples and the bare substrate (see Fig.S6, dashed lines for TDS and solid lines for the CW system). The bare substrate shows a transparency of around 95% in the 0.1 THz to 1.3 THz range due to its highly porous nature. The measurements from both TDS and CW systems prove to be in good agreement showing that both methods are well adapted for Silver Nanowires layers characterization. The samples' transmittances are decreasing with the increasing nanowire densities and are relatively flat over the measured frequency range. Additionally, the transmittance of sample C is smaller than samples B and A, similar to the optical transmittance, which we attribute to the differences in nanowire dimensions. The nanowires in samples A and B are larger than C, resulting in a smaller filling factor for the same density and thus a higher transmittance. The complex conductance of the nanowire layer as a function of ω the frequency was calculated from the measured transmittance as:[46]

$$\hat{\sigma}(\omega) = \frac{1}{Z_0}(\hat{n}_{sub} + 1) \cdot \left(\frac{\hat{E}_0(\omega)}{\hat{E}(\omega)} - 1 \right) \tag{1}$$

where $Z_0 = 377\ \Omega$ is the impedance of free space, $\hat{n}_{sub}$ is the complex refractive index of the substrate, and $\hat{E}_0(\omega)$ and $\hat{E}(\omega)$ are the complex electric field amplitudes of THz wave, transmitted through the bare substrate and the substrate with the nanowires.The complex refractive index of the substrate was extracted from a reference measurement of the filter without nanowires.The calculated conductance of the samples is shown in Fig. 3.

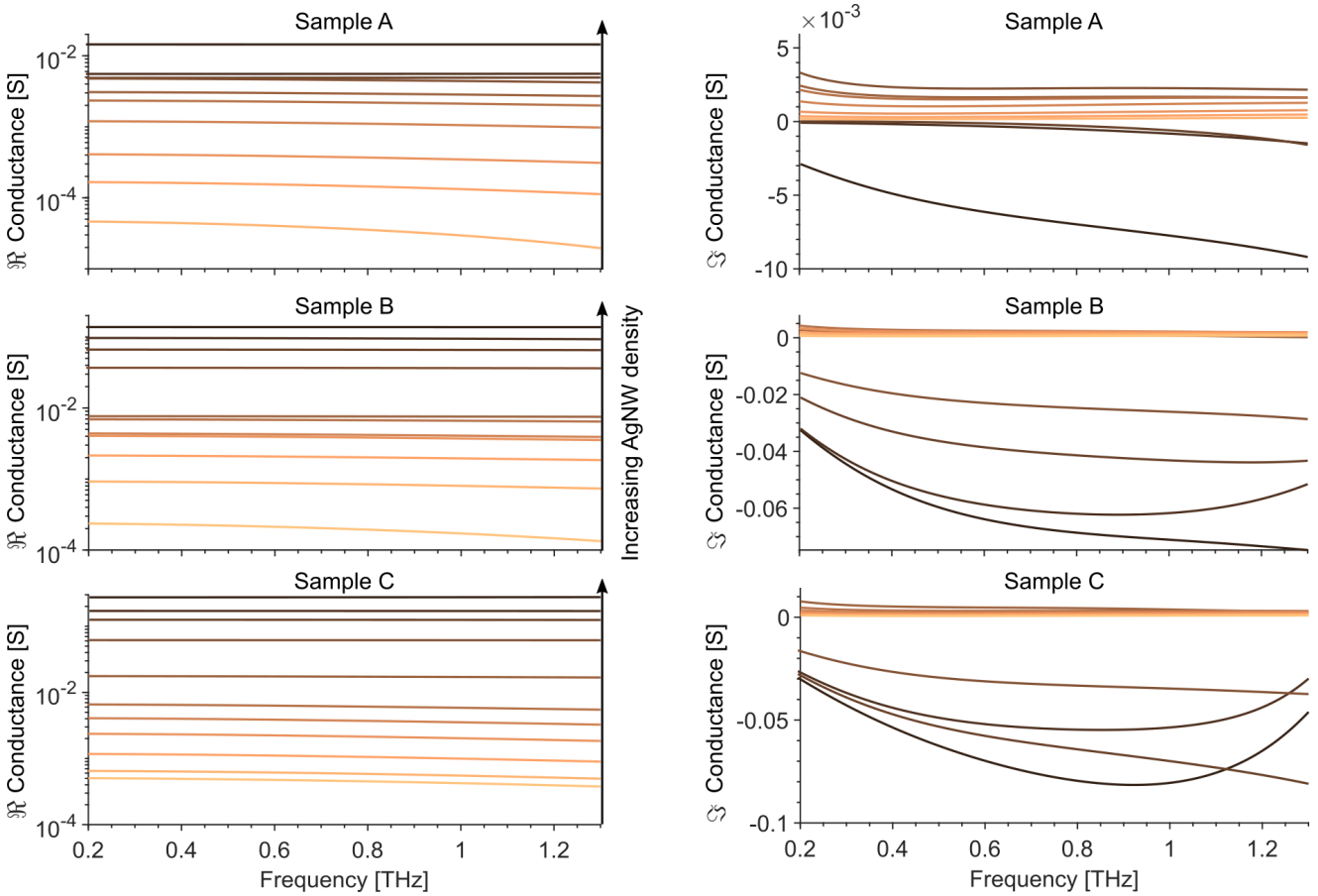

Figure 3. Real and Imaginary parts of the samples' THz conductance with different nanowire densities, calculated from the TDS measurement data according to Eq. 1.

The measured transmittance was fitted by a physical model of THz conductivity to estimate the 3D filling factor of the nanowires f and the layer thickness h. The single-scattering approximation of the Drude-Smith model was used in the form:

$$\varepsilon_{eff}(\omega) = \varepsilon_\infty - \frac{\omega_p^2}{\omega(\omega - i\gamma)}\left(1 + \frac{C_1}{1 - i\omega/\gamma}\right) \tag{2}$$

Sample	h (nm)	f	C_1	γ (Hz)
C8	1200	0.35	0	$2.45{\cdot}10^{15}$
C7	800	0.2	0	$1.4{\cdot}10^{15}$
C6	570	0.1	0	$7.0{\cdot}10^{14}$
C5	275	0.08	0	$5.6{\cdot}10^{14}$
C4	250	0.085	-0.983	$5.95{\cdot}10^{14}$
C3	180	0.08	-0.997	$5.6{\cdot}10^{14}$
C2	80	0.1	-1	$7.35{\cdot}10^{14}$
C1	80	0.11	-1	$7.7{\cdot}10^{14}$

Table 2. Drude-Smith fitting parameters for AgNW samples C

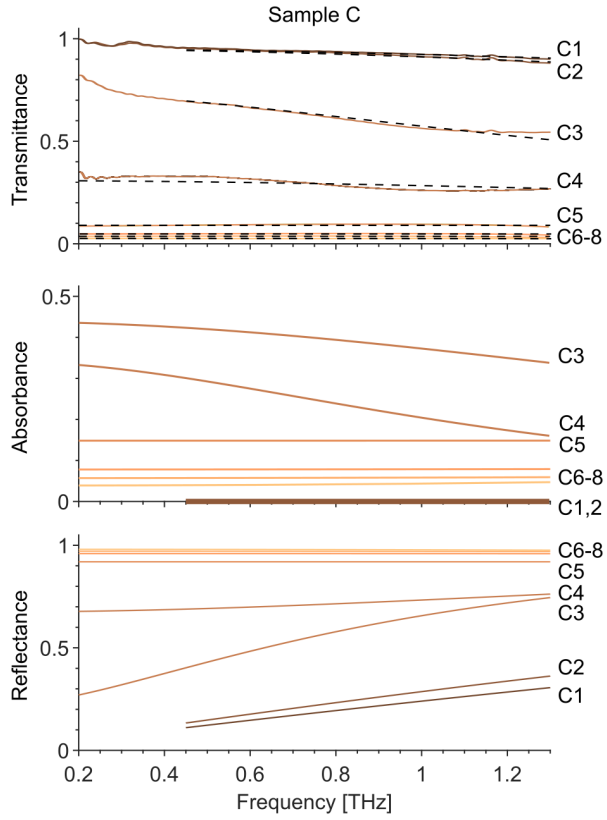

Figure 4. Transmittance (solid lines – measured, dashed – calculated), Absorbance and Reflectance (calculated) of AgNWs samples C with different nanowire densities extracted from the fitted Drude-Smith conductivity model according to (2) and Table 2.

where $\varepsilon_\infty = 0.11$, ω_p the effective plasma frequency, γ is the damping factor, C_1 the scattering parameter. The obtained fitting parameters are given in Table 2 for decreasing nanowire densities of several samples C. The absorbance and reflectance were calculated according to $A = 1 - T - R$. The calculated and fitted T, A, and R are shown in Fig. 4 for AgNW samples C with different densities.The fitted layer thicknesses h match those observed with AFM and SEM. For the samples with the lowest nanowire densities (C1 to C4), the effective plasma frequency is taken equal to the bulk silver one $\omega_{p,AG} = 1.32 \cdot 10^{16}$

rad/s. The fitted scattering parameter C_1 is close to -1, which indicates high carrier localization in the nanowires and preferential backscattering. Such behavior can be explained by the backscattering of electrons from the nanowire walls, usually observed for networks below the percolation threshold. For the samples with the highest nanowire densities (C5 to C8), the scattering parameter C_1 is set to 0, corresponding to Drude-like scattering. In this case, the conductivity corresponds to a semi-continuous metallic layer, with an effective plasma frequency taken as $\omega_p^2 = \omega_{p,Ag}^2 \cdot f$, with f the filling factor of the nanowire network. These two THz conductivity models explain the measured effective conductivity, where the imaginary part is negative or positive depending on the nanowire layer density. We would like to stress that the theoretical approach describes well the experimental results and therefore it shows that can be used for modelling/predicting THz response as a function the nanowire layer structure.

Conclusions

We have fabricated and experimentally characterized thin layers of silver nanowires in the terahertz frequency range. In particular, samples with three different nanowire geometries and increasing densities were measured in a transmission geometry by terahertz spectroscopy, both in time and frequency domains. The results obtained from the two systems are in good agreement and allow to validate both experimental methods for characterization Silver nanowires layers.We extracted the conductance of the samples from the measurements and fitted the results with a modified Drude-Smith model of conductivity. The results indicate that the samples with a low density of nanowires follow the Drude-Smith model with a backscattering coefficient close to -1,indicating high localization of electrons in the nanowires. The samples with a high density form a semi-continuous metallic layer. The layers follow a Drude-like model of conductivity with an effective plasma frequency adjusted by the 3D filling factor of the nanowires. The relatively constant conductance of the nanowire layers in a broad frequency range is of particular interest,as tunable transparent coatings are distinctly demanded for high-frequency applications. Our results pave the way toward the application of silver nanowires as a perspective material for nanoelectronic circuits, transparent and conductive coatings,and printable THz antennas, essential for future wireless communication systems.

References

1. Goliya, Y. *et al.* Next Generation Antennas Based on Screen-Printed and Transparent Silver Nanowire Films. *Adv. Opt. Mater.* **7**, 1900995, DOI: 10.1002/adom.201900995 (2019).
2. Hosako, I. *et al.* At the Dawn of a New Era in Terahertz Technology. *Proc. IEEE* **95**, 1611–1623, DOI: 10.1109/JPROC.2007.898844 (2007).
3. Pawar, A. Y., Sonawane, D. D., Erande, K. B. & Derle, D. V. Terahertz technology and its applications. *Drug Invent. Today* **5**, 157–163, DOI: 10.1016/j.dit.2013.03.009 (2013).
4. Fukunaga, K. & Picollo, M. Terahertz spectroscopy applied to the analysis of artists' materials. *Appl. Phys. A: Mater. Sci. & Process.* **100**, 591–597, DOI: 10.1007/s00339-010-5643-y (2010).
5. Akyildiz, I. F., Jornet, J. M. & Han, C. Terahertz band: Next frontier for wireless communications. *Phys. Commun.* **12**, 16–32, DOI: 10.1016/j.phycom.2014.01.006 (2014).
6. Borovkova, M. *et al.* Investigation of terahertz radiation influence on rat glial cells. *Biomed. Opt. Express* **8**, 273–280, DOI: 10.1364/BOE.8.000273 (2017).
7. Tenggara, A. P., Park, S. J., Yudistira, H. T., Ahn, Y. H. & Byun, D. Fabrication of terahertz metamaterials using electrohydrodynamic jet printing for sensitive detection of yeast. *J. Micromechanics Microengineering* **27**, 035009, DOI: 10.1088/1361-6439/aa5a9f (2017).
8. Smirnov, S. *et al.* Optically Controlled Dielectric Properties of Single-Walled Carbon Nanotubes for Terahertz Wave Applications. *Nanoscale* **10**, 12291–12296, DOI: 10.1039/c8nr03740j (2018).
9. Son, J.-H., Oh, S. J. & Cheon, H. Potential clinical applications of terahertz radiation. *J. Appl. Phys.* **125**, 190901, DOI: 10.1063/1.5080205 (2019).
10. Huang, Y., Wu, L.-S., Tang, M. & Mao, J. Design of a Beam Reconfigurable THz Antenna With Graphene-Based Switchable High-Impedance Surface. *IEEE Transactions on Nanotechnol.* **11**, 836–842, DOI: 10.1109/TNANO.2012.2202288 (2012).
11. Llatser, I. *et al.* Graphene-based nano-patch antenna for terahertz radiation. *Photonics Nanostructures - Fundamentals Appl.* **10**, 353–358, DOI: 10.1016/j.photonics.2012.05.011 (2012).
12. Tamagnone, M., Gómez-Díaz, J. S., Mosig, J. R. & Perruisseau-Carrier, J. Reconfigurable terahertz plasmonic antenna concept using a graphene stack. *Appl. Phys. Lett.* **101**, 214102, DOI: 10.1063/1.4767338 (2012).

13. Rivera-Lavado, A. *et al.* Dielectric Rod Waveguide Antenna as THz Emitter for Photomixing Devices. *IEEE Transactions on Antennas Propag.* **63**, 882–890, DOI: 10.1109/TAP.2014.2387419 (2015).

14. Komoda, N. *et al.* Printed silver nanowire antennas with low signal loss at high-frequency radio. *Nanoscale* **4**, 3148–3153, DOI: 10.1039/C2NR30485F (2012).

15. Rai, T., Dantes, P., Bahreyni, B. & Kim, W. S. A Stretchable RF Antenna With Silver Nanowires. *IEEE Electron Device Lett.* **34**, 544–546, DOI: 10.1109/LED.2013.2245626 (2013).

16. Song, L., Myers, A. C., Adams, J. J. & Zhu, Y. Stretchable and Reversibly Deformable Radio Frequency Antennas Based on Silver Nanowires. *ACS Appl. Mater. & Interfaces* **6**, 4248–4253, DOI: 10.1021/am405972e (2014).

17. Salmerón, J. F. *et al.* Properties and Printability of Inkjet and Screen-Printed Silver Patterns for RFID Antennas. *J. Electron. Mater.* **43**, 604–617, DOI: 10.1007/s11664-013-2893-4 (2014).

18. Kim, B. S. *et al.* Reversibly Stretchable, Optically Transparent Radio-Frequency Antennas Based on Wavy Ag Nanowire Networks. *ACS Appl. Mater. & Interfaces* **8**, 2582–2590, DOI: 10.1021/acsami.5b10317 (2016).

19. Sannicolo, T. *et al.* Metallic Nanowire-Based Transparent Electrodes for Next Generation Flexible Devices: A Review. *Small* **12**, 6052–6075, DOI: 10.1002/smll.201602581 (2016).

20. Lee, S. Y., Choo, M., Jung, S. & Hong, W. Optically Transparent Nano-Patterned Antennas: A Review and Future Directions. *Appl. Sci.* **8**, 901, DOI: 10.3390/app8060901 (2018).

21. Parente, M. *et al.* Simple and Fast High-Yield Synthesis of Silver Nanowires. *Nano Lett.* **20**, 5759–5764, DOI: 10.1021/acs.nanolett.0c01565 (2020).

22. Hong, J. T. *et al.* Enhanced sensitivity in THz plasmonic sensors with silver nanowires. *Sci. Reports* **8**, 1–8, DOI: 10.1038/s41598-018-33617-2 (2018).

23. Nirmalraj, P. N. *et al.* Manipulating Connectivity and Electrical Conductivity in Metallic Nanowire Networks. *Nano Lett.* **12**, 5966–5971, DOI: 10.1021/nl303416h (2012).

24. Pyo, J. B. *et al.* Floating compression of Ag nanowire networks for effective strain release of stretchable transparent electrodes. *Nanoscale* **7**, 16434–16441, DOI: 10.1039/C5NR03814F (2015).

25. Hong, J. T., Park, S. J., Park, J.-y., Lee, S. & Ahn, Y. H. Terahertz slot antenna devices fabricated on silver nanowire network films. *Opt. Mater. Express* **7**, 1679–1685, DOI: 10.1364/OME.7.001679 (2017).

26. Lefèvre, V. *Nanowires: Properties, Synthesis, and Applications* (Nova Science Publishers, 2012).

27. Anoshkin, I. V. *et al.* Resistivity and optical transmittance dependence on length and diameter of nanowires in silver nanowire layers in application to transparent conductive coatings. *Micro Nano Lett.* **11**, 343–347, DOI: 10.1049/mnl.2015.0582 (2016).

28. Ye, S., Rathmell, A. R., Chen, Z., Stewart, I. E. & Wiley, B. J. Metal Nanowire Networks: The Next Generation of Transparent Conductors. *Adv. Mater.* **26**, 6670–6687, DOI: 10.1002/adma.201402710 (2014).

29. Noh, Y.-J., Kim, S.-S., Kim, T.-W. & Na, S.-I. Cost-effective ITO-free organic solar cells with silver nanowire–PEDOT:PSS composite electrodes via a one-step spray deposition method. *Sol. Energy Mater. Sol. Cells* **120**, 226–230, DOI: 10.1016/j.solmat.2013.09.007 (2014).

30. Hoof, N., Parente, M., Baldi, A. & Rivas, J. G. Terahertz time-domain spectroscopy and near-field microscopy of transparent silver nanowire networks. *Adv. Opt. Mater.* **8**, 1900790, DOI: 10.1002/adom.201900790 (2020).

31. Langley, D. *et al.* Flexible transparent conductive materials based on silver nanowire networks: A review. *Nanotechnology* **24**, 452001, DOI: 10.1088/0957-4484/24/45/452001 (2013).

32. Xu, W. *et al.* Fabrication of Flexible Transparent Conductive Films with Silver Nanowire by Vacuum Filtration and PET Mold Transfer. *J. Mater. Sci. & Technol.* **32**, 158–161, DOI: 10.1016/j.jmst.2015.12.009 (2016).

33. Huang, Q., Al-Milaji, K. N. & Zhao, H. Inkjet Printing of Silver Nanowires for Stretchable Heaters. *ACS Appl. Nano Mater.* **1**, 4528–4536, DOI: 10.1021/acsanm.8b00830 (2018).

34. Cui, Z., Han, Y., Huang, Q., Dong, J. & Zhu, Y. Electrohydrodynamic printing of silver nanowires for flexible and stretchable electronics. *Nanoscale* **10**, 6806–6811, DOI: 10.1039/C7NR09570H (2018).

35. Li, W., Yang, S. & Shamim, A. Screen printing of silver nanowires: Balancing conductivity with transparency while maintaining flexibility and stretchability. *npj Flex. Electron.* **3**, 1–8, DOI: 10.1038/s41528-019-0057-1 (2019).

36. Kim, J. *et al.* Terahertz time-domain measurement of non-Drude conductivity in silver nanowire thin films for transparent electrode applications. *Appl. Phys. Lett.* **102**, 011109, DOI: 10.1063/1.4773179 (2013).

37. Lu, Y. C. & Chou, K. S. Tailoring of silver wires and their performance as transparent conductive coatings. *Nanotechnology* **21**, 215707, DOI: 10.1088/0957-4484/21/21/215707 (2010).

38. Hu, L., Kim, H. S., Lee, J.-Y., Peumans, P. & Cui, Y. Scalable Coating and Properties of Transparent, Flexible, Silver Nanowire Electrodes. *ACS Nano* **4**, 2955–2963, DOI: 10.1021/nn1005232 (2010).

39. Liu, C.-H. & Yu, X. Silver nanowire-based transparent, flexible, and conductive thin film. *Nanoscale Res. Lett.* **6**, 75, DOI: 10.1186/1556-276X-6-75 (2011).

40. Shi, Y. *et al.* Synthesis and Applications of Silver Nanowires for Transparent Conductive Films. *Micromachines* **10**, 330, DOI: 10.3390/mi10050330 (2019).

41. Räisänen, A. V. *et al.* Suitability of roll-to-roll reverse offset printing for mass production of millimeter-wave antennas: Progress report. In *2016 Loughborough Antennas Propagation Conference (LAPC)*, 1–5, DOI: 10.1109/LAPC.2016.7807528 (2016).

42. Nicolson, A. M. & Ross, G. F. Measurement of the Intrinsic Properties of Materials by Time-Domain Techniques. *IEEE Transactions on Instrumentation Meas.* **19**, 377–382, DOI: 10.1109/TIM.1970.4313932 (1970).

43. Dudorov, S., Lioubtchenko, D., Mallat, J. & Raisanen, A. Differential open resonator method for permittivity measurements of thin dielectric film on substrate. *IEEE Transactions on Instrumentation Meas.* **54**, 1916–1920, DOI: 10.1109/TIM.2005.853352 (2005).

44. Brown, E. R., Smith, F. W. & McIntosh, K. A. Coherent millimeter-wave generation by heterodyne conversion in low-temperature-grown GaAs photoconductors. *J. Appl. Phys.* **73**, 1480–1484, DOI: 10.1063/1.353222 (1993).

45. Deninger, A. J., Roggenbuck, A., Schindler, S. & Preu, S. 2.75 THz tuning with a triple-DFB laser system at 1550 nm and InGaAs photomixers. *J. Infrared, Millimeter, Terahertz Waves* **36**, 269–277, DOI: 10.1007/s10762-014-0125-5 (2015).

46. Tinkham, M. Energy Gap Interpretation of Experiments on Infrared Transmission through Superconducting Films. *Phys. Rev.* **104**, 845–846, DOI: 10.1103/PhysRev.104.845 (1956).

Acknowledgements

The work was supported by Horizon 2020 Grant Agreement no: 862788, by the "International Research Agendas" program of the Foundation for Polish Science co-financed by the European Union under the European Regional Development Fund (No. MAB/2018/9), and by the RUDN University Strategic Academic Leadership Program (I. S. Nefedov).

Author contributions

AP – samples preparation, writing the manuscript with input from all authors. SS – interpretation of the results, writing the manuscript with input from all authors. IN – samples characterisation AFM and SEM, UV-Vis AK – samples preparation, samples characterisation IN – performed the analytical computations PD – TDS setup adjustment DZ – TDS data processing VC – TDS measurements DB – CW system adjustment and measurements KS – CW measurements AL – CW measurements and data processing JO – supervision MK – TDS measurements supervision WK – CW measurements supervision DL – designed the study, writing the manuscript and supervision.

Competing interests

The authors declare no competing interests.

Supplementary information

The manuscript contains supplementary information.

Figures

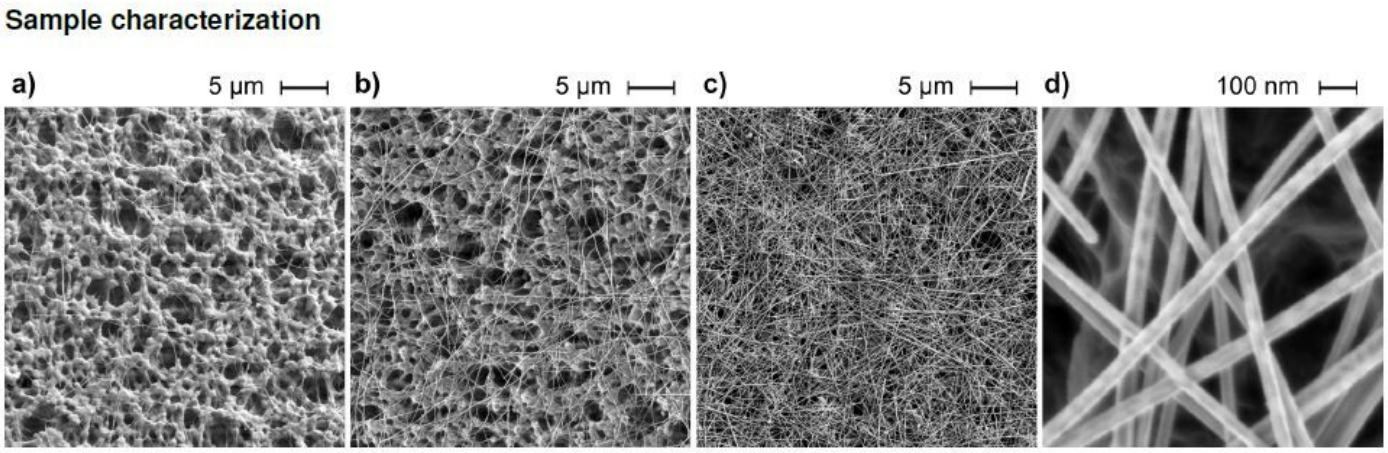

Figure 1

SEM images of AgNWs C samples with a) lowest sample density, showing individual nanowires and the morphology of the porous substrate, b) intermediate sample density at the percolation threshold, where the nanowires form a connected network, c) highest sample density with the nanowires forming a semi-continuous metallic layer, d) high magnification of c).

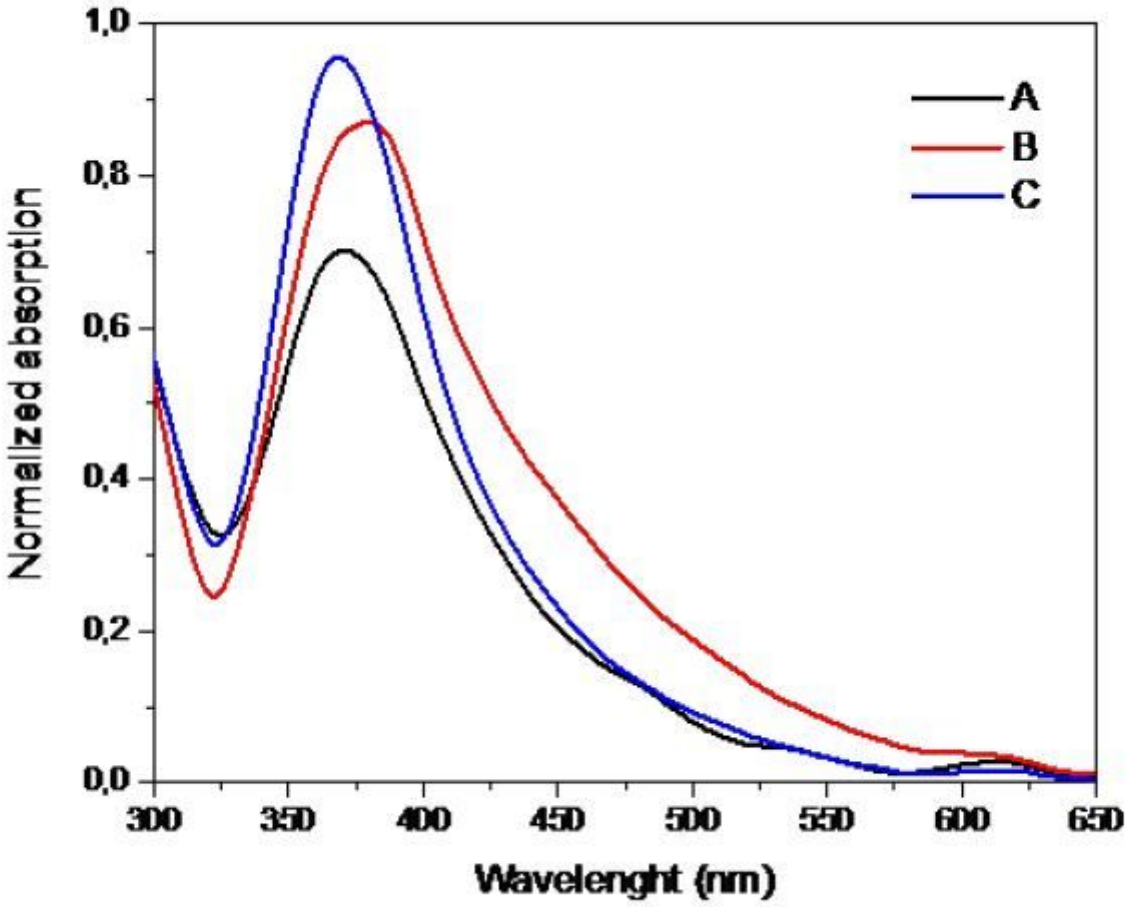

Figure 2

Optical absorbance of the three AgNW sample suspensions.

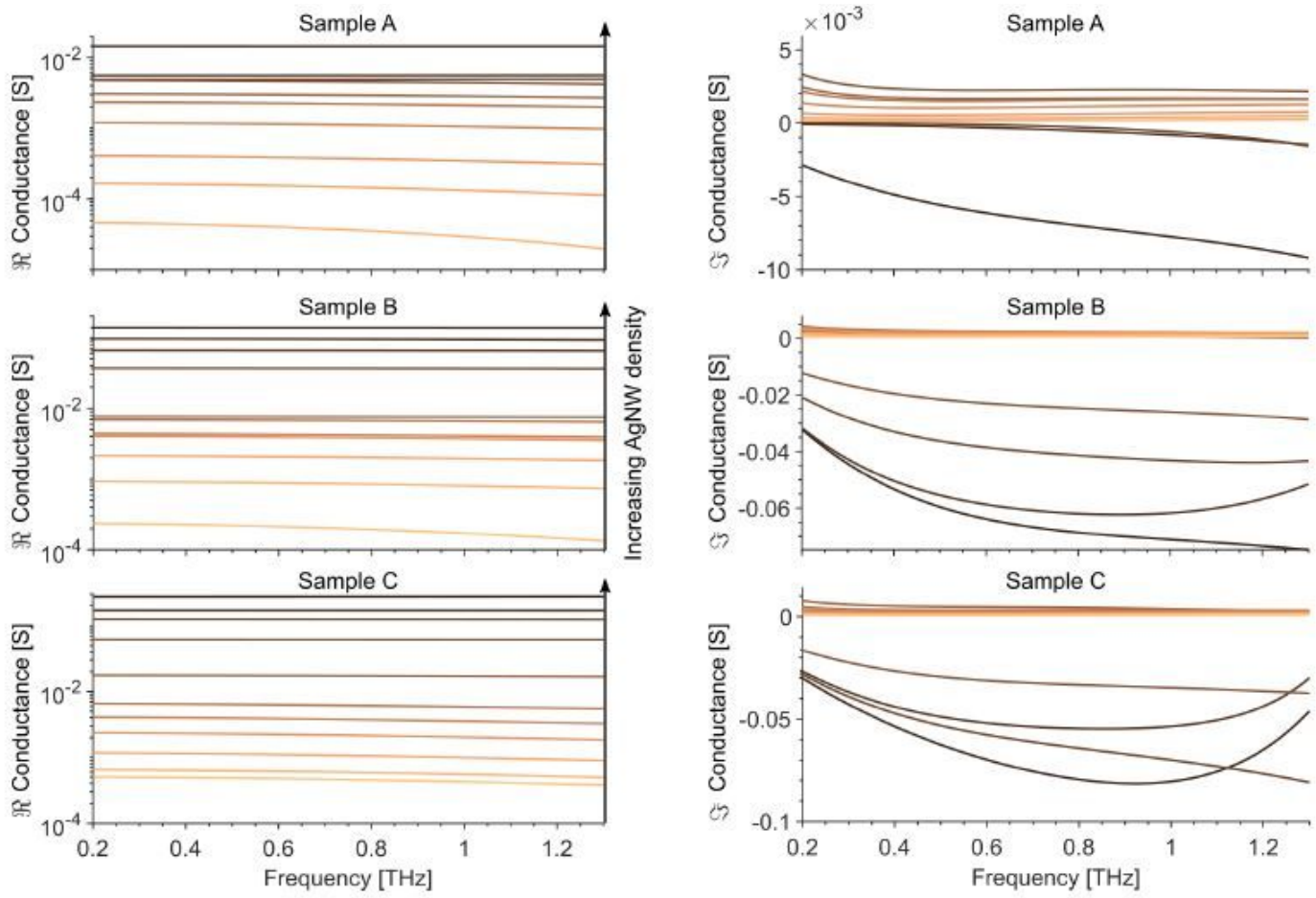

Figure 3

Real and Imaginary parts of the samples' THz conductance with different nanowire densities, calculated from the TDS measurement data according to Eq. 1.

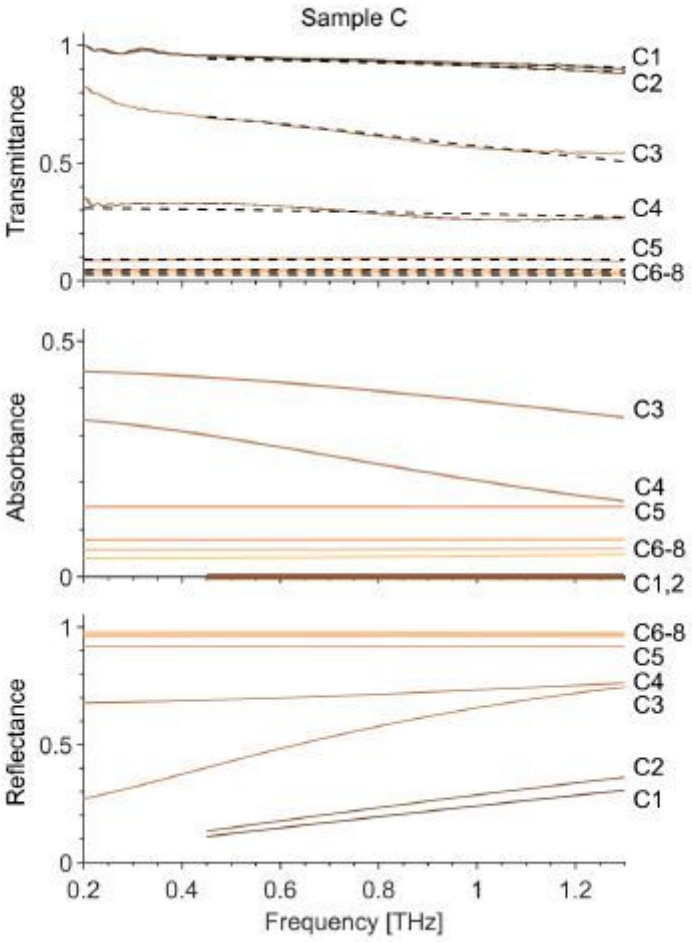

Figure 4

Transmittance (solid lines – measured, dashed – calculated), Absorbance and Reflectance (calculated) of AgNWs samples C with different nanowire densities extracted from the fitted Drude-Smith conductivity model according to (2) and Table 2.

Supplementary Files

This is a list of supplementary files associated with this preprint. Click to download.

- SuplAgNWs.pdf